LBL-19766 Rev.
c.2

Lawrence Berkeley Laboratory

UNIVERSITY OF CALIFORNIA

LAWRENCE
BERKELEY LABORATORY
NOV 4 1985
LIBRARY AND
DOCUMENTS SECTION

Materials & Molecular Research Division

Presented at the Third International Symposium on Catalyst Deactivation and Poisoning, Berkeley, CA, June 19-21, 1985

DEACTIVATION AND POISONING OF FUEL CELL CATALYSTS

P.N. Ross, Jr.

September 1985

TWO-WEEK LOAN COPY
This is a Library Circulating Copy
which may be borrowed for two weeks.

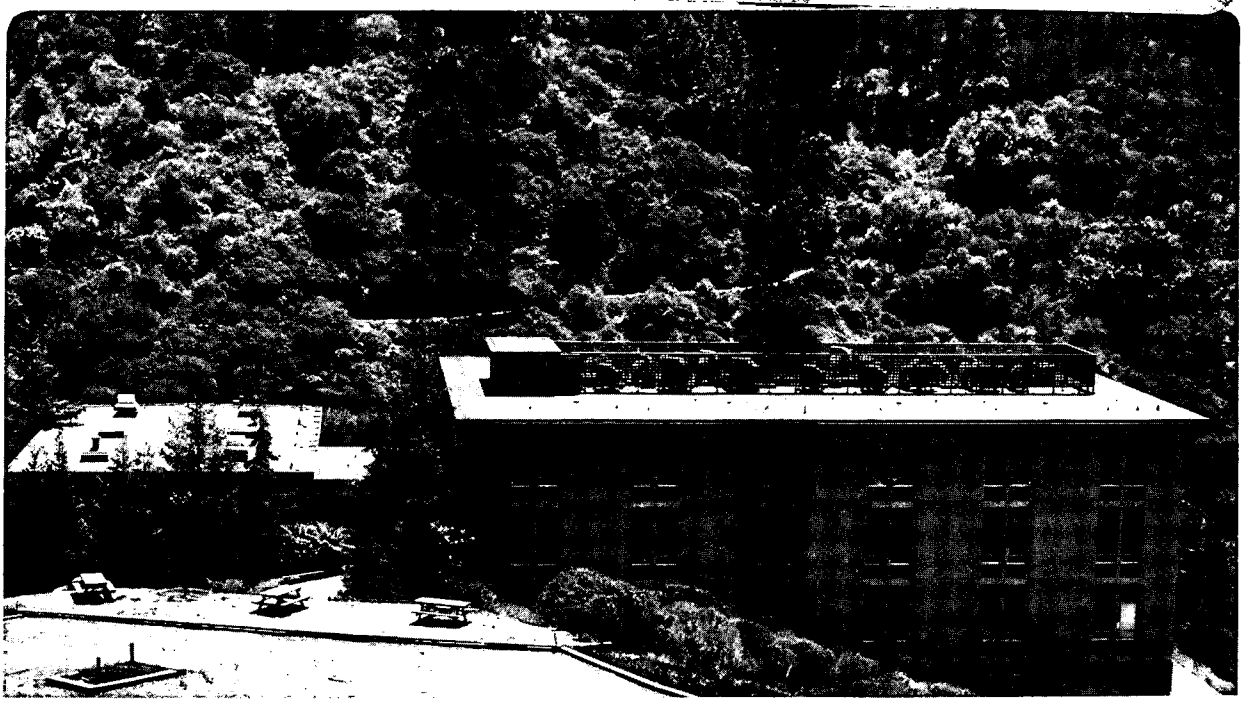

Prepared for the U.S. Department of Energy under Contract DE-AC03-76SF00098

LBL-19766 Rev.
c.2

DISCLAIMER

This document was prepared as an account of work sponsored by the United States Government. While this document is believed to contain correct information, neither the United States Government nor any agency thereof, nor the Regents of the University of California, nor any of their employees, makes any warranty, express or implied, or assumes any legal responsibility for the accuracy, completeness, or usefulness of any information, apparatus, product, or process disclosed, or represents that its use would not infringe privately owned rights. Reference herein to any specific commercial product, process, or service by its trade name, trademark, manufacturer, or otherwise, does not necessarily constitute or imply its endorsement, recommendation, or favoring by the United States Government or any agency thereof, or the Regents of the University of California. The views and opinions of authors expressed herein do not necessarily state or reflect those of the United States Government or any agency thereof or the Regents of the University of California.

DEACTIVATION AND POISONING OF FUEL CELL CATALYSTS

Philip N. Ross, Jr.

Materials and Molecular Research Division
Lawrence Berkeley Laboratory
University of California
Berkeley, CA 94720

Proceedings of 3rd International Symposium
on Catalyst Deactivation and Poisoning

University of California at Berkeley

June 19-21, 1985

1. Introduction

A fuel cell is an electrochemical energy conversion device which converts chemical to electrochemical energy without the use of an intermediate mechanical (or Carnot) cycle. At present, all fuel cell devices approaching real practice convert only hydrogen directly, and not any form of hydrocarbon. This is not a fundamental limitation but a practical limitation due to the absence of a catalyst which provides direct conversion of hydrocarbons at a practical rate (and cell potential). With the exception of special purpose fuel cells that use pure hydrogen as fuel, e.g. space and deep-sea vehicles, fuel cells have a fuel conditioning (steam reforming and water gas shifting) unit that converts a hydrocarbon fuel into a hydrogen rich gas that is fed to the electrical generating unit, as shown schematically in Fig. 1. Typical hydrocarbon fuels in use are natural gas, naptha, and methanol. Heavier fuels or gases are problematic and are the subject of research and development designed to broaden the fuel range for future fuel cell technology. In this paper, we will not discuss the problems of catalyst deactivation in the fuel conditioning unit, since these are conventional catalysts and reactors that are covered by other papers in this symposium. The discussion here will be restricted to the unique aspects of catalysts in the electrical generating unit of fuel cells.

Fuel cell catalysts suffer from deactivation and poisoning phenomena that are either identical to or strongly analogous to the processes which occur in heterogeneous catalysis. As in conventional catalytic reactors, fuel cell performance is degraded by poisoning from impurities, loss of

surface area of noble metal, and physical deterioration of the catalyst structure. Unlike conventional catalytic reactors, where some catalyst regeneration capability is usually designed into the system, the fuel cell catalyst is an integral part of the physical structure of the electrical generator, and there are at present no designs which are able to employ catalyst regeneration. Therefore, catalyst deactivation and poisoning phenomena are even more serious technological problems in fuel cells than in conventional reactors.

The deactivation and poisoning phenomena to be reviewed in detail in this paper are: the poisoning of anode (fuel electrode) catalyst by carbon monoxide; the deactivation of the cathode (air electrode) catalyst by loss of Pt dispersion; and the deactivation of the cathode by corrosion processes. The fuel cell technology discussed in the context of this phenomena is the phosphoric acid fuel cell. The operating conditions for this technology are typically 180-210°C, 95-99% acid, and in pressurized versions 50-120 psig.

The anode catalyst is Pt supported on a conductive, high area carbon black (usually Cabot Vulcan XC-72R), usually at a loading of 10 w/o. This catalyst is tolerant to some level of carbon monoxide, the level depending on temperature and pressure. Carbon monoxide poisoning has been studied extensively, including detailed adsorption studies at various temperatures and pressures. Based on these studies, predictive models have been developed that effectively predict anode tolerance to carbon monoxide.

The cathode catalyst is typically Pt supported on a graphitic carbon

black, usually a furnace black heat-treated to 2700°C. The Pt loading is typically 10 w/o, and the dispersion (or percent exposed) as-prepared is typically 30%. The loss of dispersion ("sintering") in use depends on the operational parameters, e.g. temperature, acid concentration, and electrode potential history. Relatively few fundamental studies of this phenomenon have been published, and what are available appear to contradict experience in cells. The mechanism of loss of dispersion is not well-known. The graphitic carbon support corrodes at a finite rate that is notably potential dependent. Support corrosion causes thickening of the electrolyte film between the gas pores and the catalyst particles, which in turn causes increased diffusional resistance and performance loss. Platinum corrosion (dissolution) causes loss of Pt into the separator. Support corrosion appears to be the predominant life-limiting deactivation mechanism in phosphoric acid fuel cells, while Pt corrosion is the process that limits cell voltage (and therefore power plant efficiency).

2. Background Electrochemistry

Figure 2 shows schematically the fundamental electrochemistry occurring in a fuel cell stack. The exact composition of the hydrogen stream from the fuel cell processing subsection depends on the hydrocarbon fuel in use and the conditions chosen for operation in the reformer/shift converter. With a light, clean fuel like natural gas, the stream contains exclusively hydrogen, carbon dioxide, carbon monoxide, unreacted methane, and water vapor. By manipulating the CH_4/H_2O feed ratio and the

shift converter temperature, the hydrogen stream composition can be made to vary, e.g. the CO content can be varied from a lower limit of ca. 0.5% upwards. The capital cost of the fuel processing subsection varies inversely as the CO content of the fuel. However, CO is adsorbed on the Pt catalyst but is not oxidized (electrochemically converted to CO_2) at practical potentials and therefore acts as a poison for the electrochemical conversion of the hydrogen to solvated protons. Poisoning of the anode catalyst lowers the rate at which hydrogen can be converted at a fixed potential, which means that the current and power that can be delivered at a fixed potential decreases with increasing CO content. Decreased power density in the cell stack means an increased stack size and increased capital cost. There is, therefore, an optimum trade-off to be made between fuel processor size/cost and cell stack size/cost with the carbon monoxide content as the controlling parameter. Knowledge of the reaction rate-CO content relation is essential to the systems analysis to determine the optimum operating conditions.

Protons produced at the anode are transported via the acid electrolyte to the cathode (air electrode) where they react with oxygen to form water. The product water is transported from the cell via transpiration to the reactant air stream. The reactant air stream does not contain any species known to poison the Pt catalyst. The principal deactivation processes occurring at the cathode are Pt corrosion (dissolution into the electrolyte), loss of Pt dispersion, and carbon substrate corrosion. The corrosion properties of the Pt and carbon are fundamental properties that the fuel cell engineer can control only through the choice of operating

conditions. Systems engineering considerations indicate, as usual, that the higher temperature the better, thus stressing the corrosion limits of the cell materials. The manner in which corrosion effects cell performance is, however, not well-known, but is essential towards predicting performance lifetime. In particular, corrosion of the carbon substrate for the Pt can have a number of effects on cell performance that manifest themselves in relatively short timeframes, i.e. at times one-tenth of the expected stack lifetime. To understand how this can be the case, one needs to analyze the microstructure of the catalyst layer in a working electrode, and to model the relation between the structure and performance and structure and corrosion.

The microstructure of a phosphoric acid fuel cell electrode is shown in the diagram of Fig. 3. The authoritative treatment of transport processes in this type of electrode was by Cutlip and Iczkowski (1). The electrochemical reactions of hydrogen and oxygen occur only at the Pt surface, and is a "three-body" reaction between dissolved gaseous molecules and either water or solvated protons on the Pt surface. The electrons generated/consumed in this reaction must flow to/from the current collector to the Pt particles through the carbon substrate. Oxygen from the air (or hydrogen from the fuel gas) is transported to the reaction site via a serial diffusion path: molecular (and Knudsen) diffusion through gas pores formed in the layer by Teflon, dissolution into the electrolyte, and diffusion of dissolved gas to the Pt surface through the electrolyte "film". It is clear that corrosion of the carbon substrate can, in principle, have an effect on these transport processes

that might be incremental, rather than catastrophic, in nature. For example, corrosion of the carbon may break the current path for some agglomerates, resulting in electrical isolation of some catalyst.

3. The Poisoning of Hydrogen Oxidation by Carbon Monoxide

The generally accepted mechanism for the anodic oxidation of hydrogen at Pt surfaces in acid electrolyte is the so-called Tafel-Volmer mechanism (2),

$$H_2 + 2M \rightleftharpoons 2\ MH$$

$$2MH + 2\ H_2O \rightleftharpoons 2M + 2H_3O^+$$

with the dissociation of molecular hydrogen as the rate-determining step. Carbon monoxide adsorption on the surface blocks sites available for dissociation, and may have non-local effects on the rate of dissociation at neighboring sites. Since the dissociation step was rate determining, Ross and Stonehart (3) studied the effect of CO poisoning on the rate of H_2-D_2 exchange on Pt surfaces in order to understand the details of CO poisoning of the dissociation reaction itself. They reasoned that since the accepted mechanism for the H_2-D_2 exchange reaction on Pt surfaces was the Bonhoeffer-Farkas sequence,

$$H_2 + D_2 + 4M \rightleftharpoons 2MH + 2MD \rightleftharpoons 4M + 2HD$$

with the dissociation of molecular hydrogen rate-determining, the mechanism of poisoning of this reaction should be the same as for anodic oxidation of hydrogen. Ross and Stonehart used an all-glass apparatus similar in design to that reported by Breakespeare, et al. (4), depicted in Fig. 4. A mass-spectrometer connected to the reactor enabled them to measure via thermal desorption spectroscopy (TDS) both the CO coverage and the fraction of hydrogen sites covered by CO in the same experiment. An example of TDS spectra and this determination is shown in Fig. 5. Dosing the chamber with CO for 100 Langmuir exposure at ambient temperature was used to determine the CO signal for saturation coverage. The coverage of CO at any other condition was simply the ratio of the observed CO signal to the saturation signal. The effect of CO on the kinetics of equilibration was determined by pre-dosing the clean wire with CO, pumping out the CO, then introducing an H_2/D_2 mixture for rate measurement. After the rate measurement, the equilibrated gas mixture was pumped out, and the filament flashed, recording the mass 2,3,4 and 28 peaks simultaneously. There resulted a point for point relation between rate and both the number of available adsorption sites (Θ_H^{CO}) and the fractional coverage by CO (Θ_{CO}). The observed correlation between equilibration rate and the fraction of adsorption sites poisoned ($1-\Theta_H^{CO}$) is shown in Fig. 6. The solid line is the correlation for an ideal (energetically homogeneous) surface with the dissociation rate

proportional to the square of the number of available sites. Even though the data fit the ideal rate expression rather well over the range of CO coverage examined, there is little doubt that the surface is in fact energetically heterogeneous. The CO TDS spectra clearly showed a sequential formation of less strongly bound forms at higher coverages. It would be expected that the hydrogen chemisorption sites with the highest adsorption energy are poisoned first, followed by sites with successively higher heats of adsorption as the coverage increases. This would be expected to give rise to an activation energy which increases with increasing coverage, but this was not the case. The explanation lies in the fact that the dissociation of hydrogen on Pt is essentially activationless, so changes in the heat of adsorption have very little effect on the rate, i.e. the poisoning effect is predominantly via site elimination.

Stonehart and co-workers (5-8) extended the study of CO poisoning to the anodic oxidation of hydrogen using comparable methodology to that used in the study of H_2-D_2 exchange. To obtain the kind of coverage data obtained by TDS, they used linear sweep voltammetry (the interested catalytic chemist may wish to consult the description of this technique for these purposes by Stonehart and Ross (9)). An example of the use of this technique to measure the fractional coverage CO and the fraction of hydrogen sites poisoned simultaneously is shown in Fig. 7. The coverages measured at 145°C in 96% H_3PO_4 are shown in Fig. 8. as a function of CO partial pressure in hydrogen. The sum of the fraction of sites covered and the fraction of sites available was near unity for all CO pressures

except for singular behavior around 0.02 atm. This singularity was attributed to co-adsorption of CO and anions which depressed the hydrogen adsorption more than expected from the CO coverage. This point has not been investigated further. From a practical prospective, it is interesting to note that the coverage throughout the range of CO concentration from a reformer/shift converter is quite high at this temperature, e.g. at least 50% coverage. The ratios of the rate in the presence of CO to the rate in pure hydrogen (at the same temperature) are shown in Fig. 9 as a function of CO coverage. This figure combines the kinetic measurements of Kohlmayr and Stonehart (5) and the later measurements by Ross (10). Kohlmayr and Stonehart made their kinetic measurements by a potentiodynamic technique that was criticized by Breiter (11). Ross used the conventional rotating disk method for kinetic measurements and found CO effects consistent with the results reported by Kohlmayr and Stonehart (5). As was the case for the H_2-D_2 exchange reaction, the data are well represented by the ideal rate expression for dual-site elimination, except at high coverages of CO. The high coverage data can be explained by the additional observation that in this region ($\Theta_{CO} + \Theta_H^{CO}$) is not constant, and that a fraction (ca. 3%) of the Pt surface remains active even at saturation coverage by CO.

The results described so far for CO poisoning were all obtained using smooth polycrystalline Pt surfaces, e.g. wires, foils and disks. The real-world catalyst is supported Pt at fairly high dispersion (30% exposed), and it was important to establish that the CO poisoning of real

catalyst is at least parametrically similar. This was established in the work of Vogel, et al. (7), who also pointed out that the crystallite size independence of CO poisoning was consistent with previous findings that hydrogen oxidation on Pt catalysts (in acid electrolyte) is a facile reaction.

Ross and Stonehart (8) measured CO coverages on Pt over the expected range of cell temperatures and CO partial pressures expected from a reformer/shift converter. Together with the parametric relation established by the data in Fig. 8, these coverages have enabled fuel cell system engineers to establish the optimum operating conditions in the fuel processor (for the case of methane or naptha) leading to minimum cost of the total system.

None of the publications on CO poisoning of Pt which served as the source of the material presented above discussed either the dynamics of CO poisoning or long-term "aging" phenomena that might be associated with CO. This author is not aware of work in journal literature which discusses these subjects, although there are reports from government contracts containing some relevant information. Practically speaking, CO poisoning is essentially instantaneous, in that anode polarization increases as soon as a CO/H_2 mixture is switched for pure hydrogen. The reverse is also observed, which is expected, since fuel cell temperatures (ca. 160-190°C) are well above the desorption temperature (ca. 130°C) of CO from Pt surfaces. Very little is known about long-term aging, but anodes have been reported to operate for 20,000 hrs. without significant loss in catalyst activity (12).

4. Loss of Pt Dispersion

A detailed discussion of the processes occurring in the loss of metal dispersion of supported metal catalysts, more colloquially referred to as "sintering", has been given by another speaker in the Symposium. In this paper, we will focus on the principle differences that distinguish sintering of a supported Pt catalyst in a liquid environment from thermal sintering in vacuum or in a gaseous environment. There are two general mechanisms usually considered in the analysis of sintering, the coalescence of metal particles colliding during migration on the support, and the transport of atoms from small particles to large particles similar to the Ostwald ripening of colloidal solutions. The first process is analogous to a two-dimensional Brownian motion of metal particles on the support surface, with random collisions and subsequent coalescence. Rate expressions for the rate of particle size growth are usually derived as extensions of the Smoluchowski (13) coagulation theory. The Ostwald ripening model for thermal sintering is usually interpreted as occurring via ad-atoms or ad-molecules hopping from small particles onto the support surface, migrating across the support to larger particles and there incorporated. The transfer of atoms from a particle onto the support is a highly activated process, e.g. Wynblatt and Gjostein (14) reported an activation energy of ca. 100 kcal for this step for Pt supported on alumina, and might be expected to occur only at relatively high temperature. The corresponding Ostwald ripening mechanism for an electrocatalyst is depicted in Fig. 10. In an

electrocatalyst, the Ostwald ripening mechanism can occur via ionic species either directly through solution or by surface diffusion. The ionic species would be the solvated metal ion, and the net process is really dissolution-deposition driven by the effect of curvature of the metal surface on the metal/ion potential (15). The electrical potential gradient at the surface replaces in effect the thermal energy required to remove metal atoms from the surface, so that one might expect Ostwald ripening to occur for electrocatalysts even at low (<200°C) temperatures. The dissolution-deposition process will clearly be potential dependent, which make it a relatively easy mechanism to identify.

Bett and co-workers (16-18) studied the sintering of Pt on carbon fuel cell catalyst in both gas-phase and liquid-phase environments. At the same temperature, the rate in all the liquid media were at least an order of magnitude higher than in vacuum or inert atmosphere. Surprisingly, the rate did not change dramatically between polar and non-polar solvents, nor was the rate appreciably different in electrolytes. Consistent with these observations was the result that the sintering in phosphoric acid at typical fuel cell conditions was not potential dependent (!). Based on an analysis of the dependence of the sintering rate on Pt loading, Bett, et al. concluded that an Ostwald ripening process was occurring, but via adatoms and not solvated ions, i.e. an exact equivalent of the thermal sintering of supported metals in the gas-phase. They suggested that liquids act as a bridge for the transfer of Pt atoms from particles to the support, but were unable to provide a more detailed picture of the nature of this "bridge". Unfortunately,

there have been virtually no follow-on studies of Pt sintering that might clarify the vague picture left by Bett and co-workers.

Although the mechanism of the loss of Pt dispersion is not well-known, the practical consequences of the phenomenon are. Fuel cell developers have tried to reduce the rate of loss by various means, mostly by modification of the carbon surface, but none have been found to have a lasting effect. Post-mortem analysis of test cells has resulted in an accumulation of a substantial compilation of area vs. time data that is not readily accessible to outside investigators. Some general conclusions can be drawn from the body of reports on DOE sponsored studies: the Pt area on anodes is generally much higher than the Pt area on cathodes from the same cells, in conflict with the observation of potential independence by Bett and co-workers; the greatest area loss occurs within the first 1000 hrs. of life, with a very slow (e.g. 1 m^2/g per 1000 hrs.) rate of loss thereafter; the Pt area at cathode at the end-of-life time of 40,000 hrs. should be 30-40 m^2/g; fuel cell developers do not indicate Pt area loss as a life-limiting factor for present technology.

5. Deactivation by Corrosion Processes

There are primarily two corrosion processes that cause deactivation of fuel cell catalysts, Pt corrosion (dissolution) and carbon support corrosion. Of the two, Pt dissolution is the more obvious in terms of its direct relation to electrocatalytic activity. The solubility of Pt can be expected to be a function of acid type (anion), concentration,

temperature, and electrode potential. One might also expect an effect of Pt crystallite size on solubility, as predicted by the Kelvin equation (19). There may also be effects of impurities in the electrolyte on solubility, e.g. anions like Cl^- that have a complexing effect, or large cations that may have a salting-out effect. The measurement of Pt solubility is experimentally difficult and tedious and it is not surprising that there is very little data. The most reliable to date appears to be that reported by Bindra, Clouser and Yeager (20), reproduced in Fig. 11. The potential dependence is Nernstian, corresponding to Pt in the divalent state in solution. The effect of acid concentration and crystallite size on solubility was not measured, nor has there been a study of the effect of impurities. We can see what the consequences of these levels of Pt solubility might be for various deactivation processes by use of flux calculations. Two flux calculations using this solubility data are shown in Fig. 12. The first models the Ostwald ripening process of Pt particle size growth via dissolution-deposition; at a cathode operating potential of 0.75 V (vs. the hydrogen electrode) a Pt solubility of ca. 10^{-8} M results in a Pt flux from small particles to large of ca. 10^{13} atoms cm^{-2} sec^{-1}. This is the same order of magnitude as the flux rate of Pt ions calculated from the sintering rate data of Bett, et al. (17), clearly indicating the viability of dissolution-deposition mechanism of particle growth. The second calculation shown is the rate of loss of Pt from the cathode to the anode, by dissolution, diffusion through the matrix (electrolyte), and deposition at the anode. At 0.75 V, the rate of loss is acceptable

since the beginning of life Pt loading is ca. 0.5 mg Pt cm^{-2}. However, since the solubility increases by an order of magnitude for an increase in cathode potential of only ca. 50 mV, the rate of loss is unacceptable for sustained operation at cathode potentials above 0.8 V. This loss mechanism puts an upper limit on the thermal efficiency of phosphoric acid fuel cell power plants. In addition, operation of the fuel cell in a "hot-standby" condition at open circuit can be disastrous in terms of Pt loss. Air open circuit potentials in cathodes are typically 0.9-0.95 V; at these potentials Pt solubility is ca. 10^{-4} (!), and the Pt flux from the cathode is ca. $7x10^{-6}$ g cm^{-2} hr^{-1}, which means half the Pt would be lost in only 40 hrs. at open circuit. Therefore, this loss mechanism puts real constraints on the operating procedures for fuel cell power plants, i.e. methods must be devised to avoid extended stand at hot open circuit.

Post-mortem analysis of test cells has been consistent with the trends indicated by the above flux calculations of Pt loss. Hitachi recently reported (21) loss of 60% of the Pt from a cathode operated for 100 hrs. at 0.9 V (vs. the hydrogen electrode), or a flux rate of ca. $3.6x10^{-6}$ g cm^{-2} hr^{-1}, in reasonable agreement with the flux calculated from the solubility data of Bindra, et al. Little or no Pt was lost in this time period below 0.7 V, also in agreement with the calculations. There have been occasional reports (22,23) of significant Pt loss even from cathodes operated continuously at potentials in the 0.6-0.7 V range. It is probably the case that this loss occurred either during start-up, if a start-up procedure was employed using heating at open-circuit with air on

the cathode, or the loss came from catalyst aggregates that were electrically isolated (by Teflon) from the current collector so that they were, in effect, at hot open circuit potential. The effect of impurities in the electrolyte on Pt solubility, or the possibility of electrolyte additives for suppression of solubility remain to be determined.

The deactivation of electrodes due to support corrosion is a less direct effect than Pt corrosion, and the manifestation of the effect is more difficult to observe. From the model structure of the gas-diffusion electrode described in Section 2, it is anticipated that corrosion of the carbon support would cause thickening of the electrolyte "film" in the wetted pores containing catalyst, leading to increased diffusional resistance and performance degradation. It is unclear, however, how much corrosion must occur before this "film-thickening" begins, and whether the effect will occur gradually or rather exhibit critical threshold behavior, with rapid collapse of the gas-diffusion structure at some critical point. In addition to the "film-thickening" mechanism, there are at least two other mechanisms by which support corrosion may degrade catalytic activity. The support must carry the electrical current from the Pt particles to the current collector, and corrosion of the carbon can cause loss of carbon-carbon contact and electrical isolation of aggregates of catalyst. Support corrosion may also exacerbate the rate loss of Pt dispersion, either as a result of increased Pt particle mobility on the surface or simply as a reduction in the distance between stationary particles. At present, the extent to which any of these deactivation mechanisms apply to the performance decay of cathodes is not

known.

There have been a number of studies of the corrosion rate of various carbon blacks in phosphoric acid at fuel cell type conditions, and reviews of the data on the subject can be found in a recent proceedings volume (24). Corrosion rates of various carbon supports are, therefore, reasonably well-known. What is unknown at present is how low does the rate have to be to achieve the commercially desired life-time. There are no published studies known to this author which establish a relation between support corrosion rate and electrode life-time, although it is certainly the case that fuel cell developers have compiled extensive post-mortem data and may have established such correlations to their satisfaction. Occasionally, contract reports from developers provide a "trickle" of data, such as the recent report from Energy Research Corporation (25). Endurance testing was reported comparing electrodes made from two different carbon blacks whose corrosion rates differed by approximately a factor of five. However, after 14,000 hrs. of operation at ca. 0.65 V, the rate of performance decay was reported to be the same, indicating that at these conditions at least support corrosion was not contributing to (gradual) performance loss. Operation at higher potentials may lead to different conclusions, as seems to be the case in reports to EPRI (26). For some time, Vulcan XC 72R carbon black has been the standard support material for fuel cell catalysts, and is still the preferred support for catalysts used at the hydrogen electrode. It appears from recent reports that this carbon will not provide acceptable life-time for the electric utility fuel cell applications and that

developers are seeking a support with a corrosion rate nearly an order of magnitude lower than Vulcan.

ACKNOWLEDGMENT

This work was supported by the Electric Power Research Institute under Contract No. RP 1676-2 through an agreement with the Department of Energy under Contract No. DE-AC03-76SF0098.

References

1.) M. Cutlip and R. Iczkowski, J. Electrochem. Soc.,

2.) K. Vetter, "Electrochemical Kinetics," Academic Press, New York and London, 1967, pp. 516 ff.

3.) P. Ross and P. Stonehart, J. Catalysis, 35 (1974) 391.

4.) R. Breakspeare, D. Eley and P. Norton, J. Catalysis, 27 (1972) 215.

5.) P. Stonehart and G. Kohlmayr, Electrochim. Acta, 17 (1972) 369.

6.) G. Kohlmayr and P. Stonehart, Electrochim. Acta, 18 (1972) 211.

7.) W. Vogel, J. Lundquist, P. Ross and P. Stonehart, Electrochim. Acta, 20 (1975) 79.

8.) P. Ross and P. Stonehart, Electrochim. Acta, 21

(1976) 441.

9.) P. Stonehart and P. Ross, Catal. Rev. Sci. Eng., 12 (1975) 1.

10.) P. Ross, Proceeding of Symposium on the Electrocatalysis of Fuel Cell Reactions, The Electrochemical Society, Princeton, NJ, 1979, pp. 169-202.

11.) M. Breiter, J. Electroanal. Chem., 65 (1975) 623.

12.) L. Christner, Energy Research Corporation, Danbury, CT, private communication, 1984.

13.) M. Smoluchowski, Z. Phy. Chem., 92 (1918) 129.

14.) P. Wynblatt and N. Gijostein, Prog. Sol. State Chem., 9 (1975) 21.

15.) W. Pleith, Surf. Sci., 156 (1985) 530 and references therein.

16.) J. Bett, K. Kinoshita and P. Stonehart, J. Catalysis, 35 (1974) 307.

17.) J. Bett, K. Kinoshita and P. Stonehart, J. Catalysis, 41 (1976) 124.

18.) K. Kinoshita, J. Bett and P. Stonehart, in Sintering and Catalysis, G. Kuczinski ed., Plenum Press, New York, 1975, p 117 ff.

19.) A. Adamson, "Physical Chemistry of Surfaces," Wiley-Interscience, New York, 1960, p 56.

20.) P. Bindra, S. Clouser, and E. Yeager, J. Electrochem. Soc., 126 (1979) 1631.

21.) Y. Yoshioka, Y. Tsutsumi, and T. Mori in 1985 Fuel Cell Seminar, Courtesy Associates, Washington 1985, pp. 43-46.

22.) K. Usami, Y. Hamasaki, S. Matsuda, I. Hirata and K. Kishida, loc. cit., pp. 35-38.

23.) J. Feret, Interim Report to NASA Lewis on Contract No. DEN3-290.

24.) Proceedings of the Symposium on "The Electrochemistry of Carbon," S. Sarangapani, J. Akridge and B. Schumm, The Electrochemical Society, Princeton, NJ, 1984.

25.) A. Kush, L. Christner and P. Yeh, in 1985 Fuel Cell Seminar, Courtesy Associates, Washington, 1985, pp. 56-59.

26.) A.J. Appleby, private communication, 1984.

Figure Captions

Fig. 1. A fuel cell power plant consists of three subsystems: a fuel processor for reforming the hydrocarbon fuel to a hydrogen fuel; an electrical generating power unit (cell stacks); and a dc-ac power conditioner.

Fig. 2. Basic electrochemistry of hydrogen-oxygen fuel cells with acid electrolyte. Hydrogen molecules are oxidized at the anode producing solvated protons; protons migrate to the cathode where they react with oxygen molecules to form water; electrons flow through the external circuit to complete the loop.

Fig. 3a. Detailed geometric structure of a fuel cell gas-diffusion electrode; the porous backing is a fibrous graphite material impregnated with Teflon; the catalyst layers contain the platinized carbon catalyst wetted with electrolyte interspersed in Teflon fibers that form gas channels allowing diffusion of gas from the backing into the catalyst layer. 3b. Transport processes occurring in the structure of 3a. From R. Iczkowski and M. Cutlip (1), with permission from the Electrochem. Soc.

Fig. 4. Pt-wire reactor for the measurement of H_2-D_2 equilibration rates and for thermal spectroscopy of hydrogen and carbon monoxide from the wire surface.

1 - Au plated Ta feedthrus

2 - Pt wire

3 - Au plated Pt/Pt-10% Rh thermocouple

4 - Au plated Ta foil leak

Fig. 5. Characteristic mass spectrometer traces for linear heating of a Pt-wire dosed sequentially with carbon monoxide and hydrogen. 1 - Mass 2 trace from clean surface; 2 - Mass 2 trace from a CO poisoned surface.

Fig. 6. Correlation between the relative rate of equilibration on the CO poisoned surface and the fraction of hydrogen chemisorption sites poisoned. From P. Ross and P. Stonehart (3), with permission from Academic Press (Θ^{H}_{CO}).

Fig. 7. Cyclic voltammogram for a Pt electrode (- - -) before and (——) after exposure to 10% CD/H_2 gas in 96% H_3PO_4 at 135°C. Sweep rate was 0.086 V/s. From. G. Kohlmayr and P. Stonehart (5) with permission from Pergamon Press.

Fig. 8. Equilibrium coverages of CO (Θ_{CO}) and hydrogen (Θ_H) on Pt at 135°C in 96% H_3PO_4 as

a function of CO partial pressure in hydrogen.

Fig. 9. Correlation of relative rate at clean and CO poisoned Pt surfaces with the fraction of hydrogen chemisorption sites poisoned. From Vogel, et al. (7), with permission from Pergamon Press.

Fig. 10. Representations of the Ostwald ripening mechanism for loss of Pt dispersion.

Fig. 11. Measured Pt Solubility in 96% H_3PO_4 as a Function of Potential. Data of Bindra, et al. (20) with permission of The Electrochemical Society.

Fig. 12. Model Calculations of Pt Fluxes from Solubility of Bindra, et al. (20).

FUEL CELL POWER PLANT

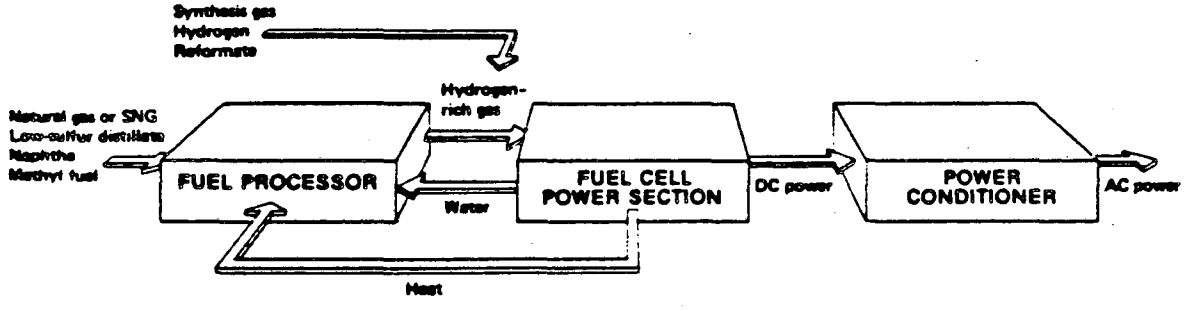

Fig. 1

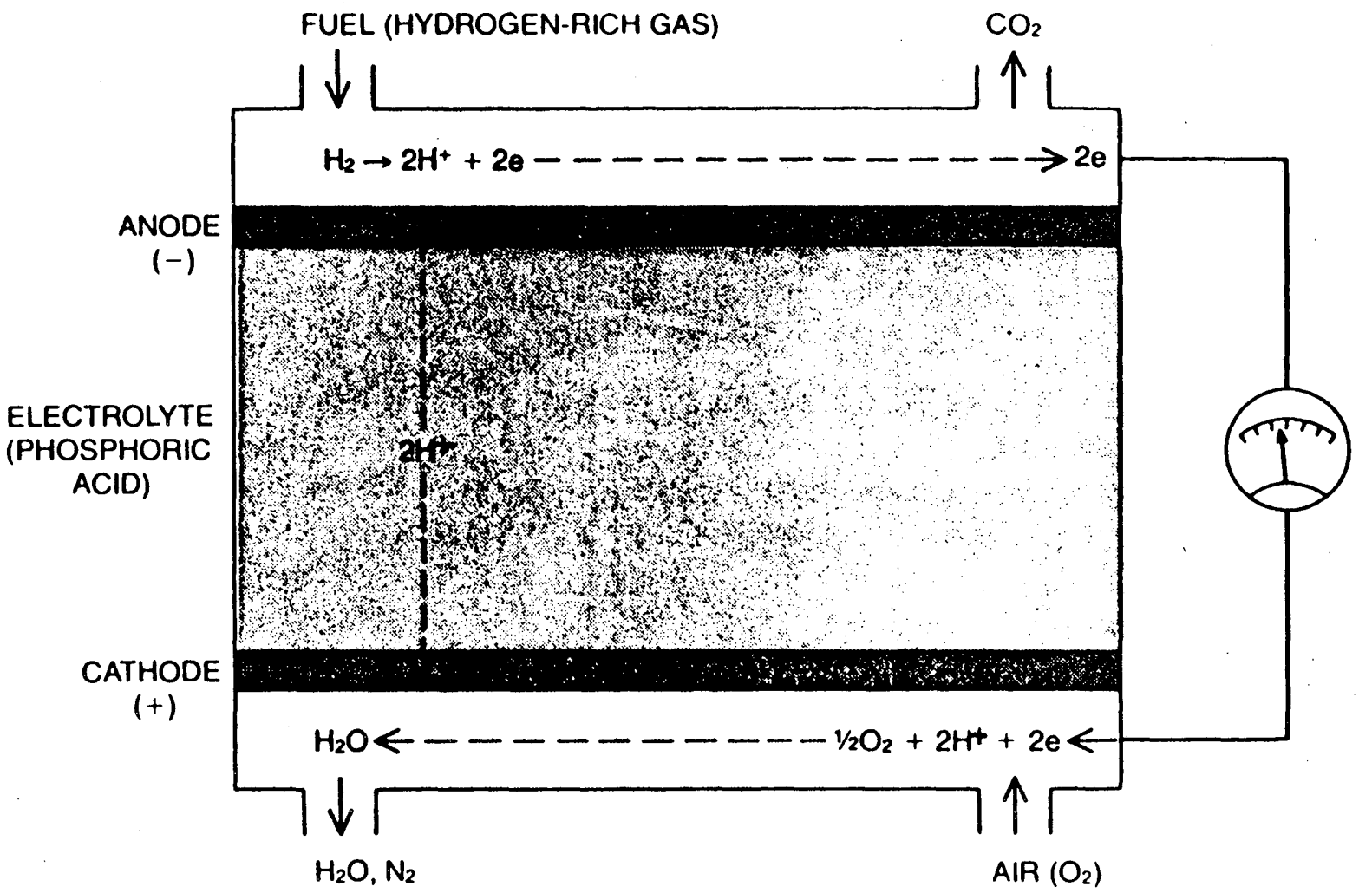

XBL 859-3979

Fig. 2

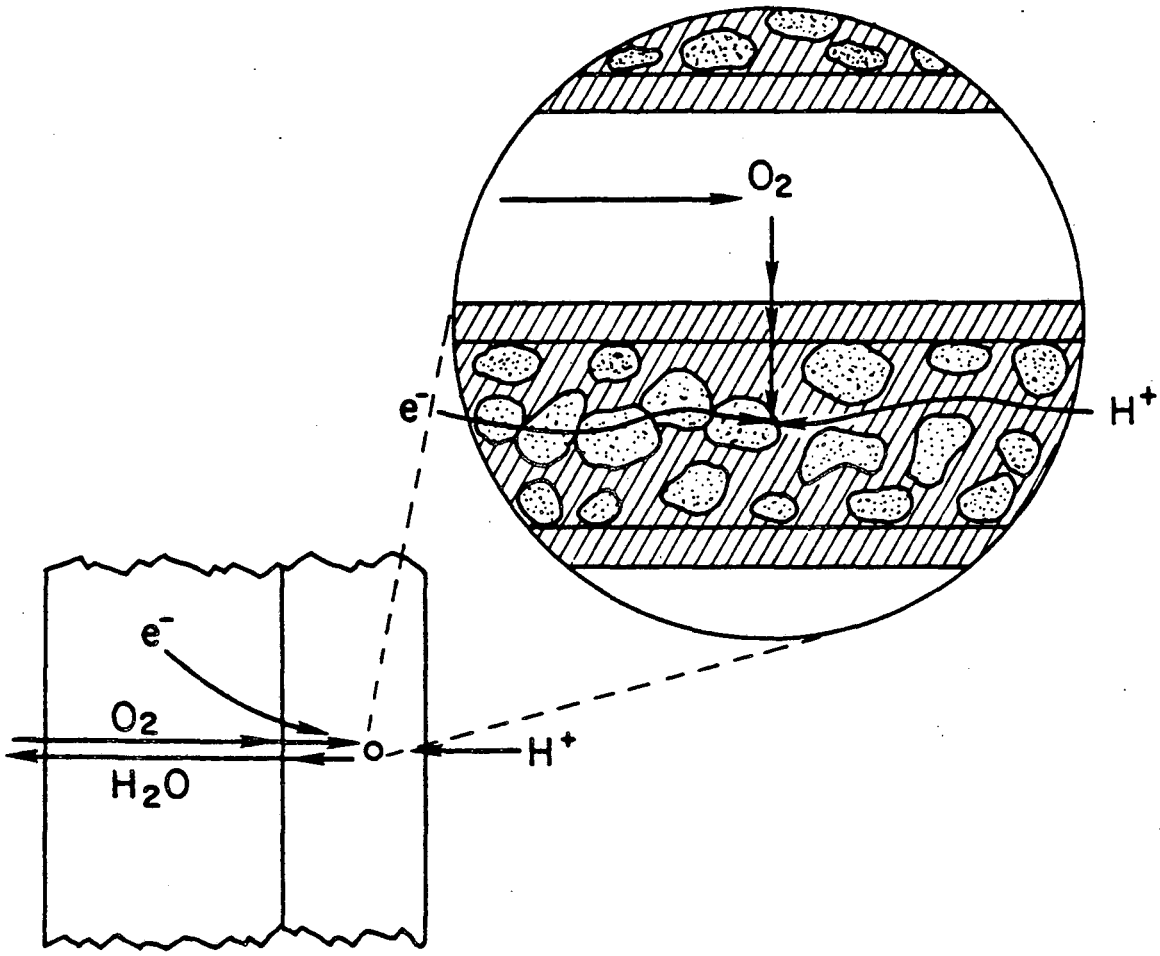

Fig. 3a

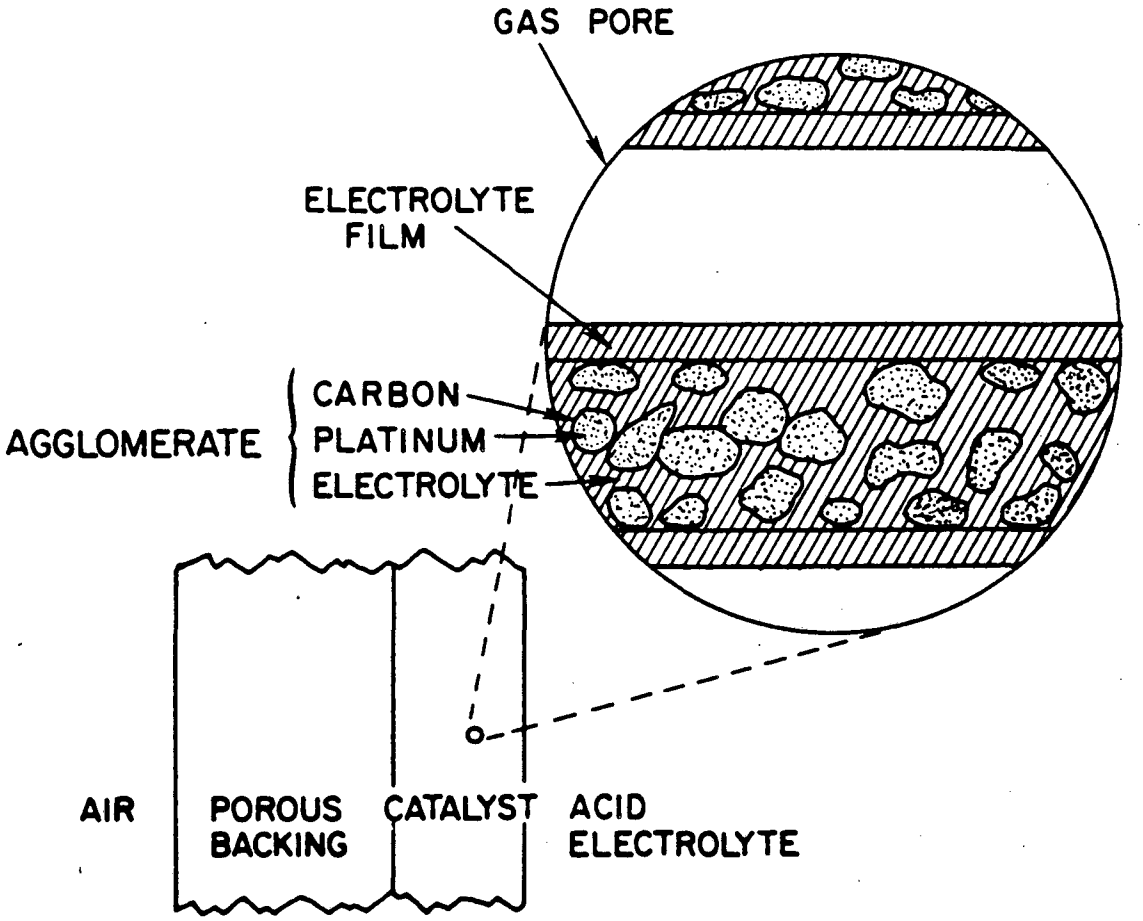
GAS PORE
ELECTROLYTE FILM
AGGLOMERATE
CARBON
PLATINUM
ELECTROLYTE
AIR
POROUS BACKING
CATALYST
ACID ELECTROLYTE

Fig. 3b

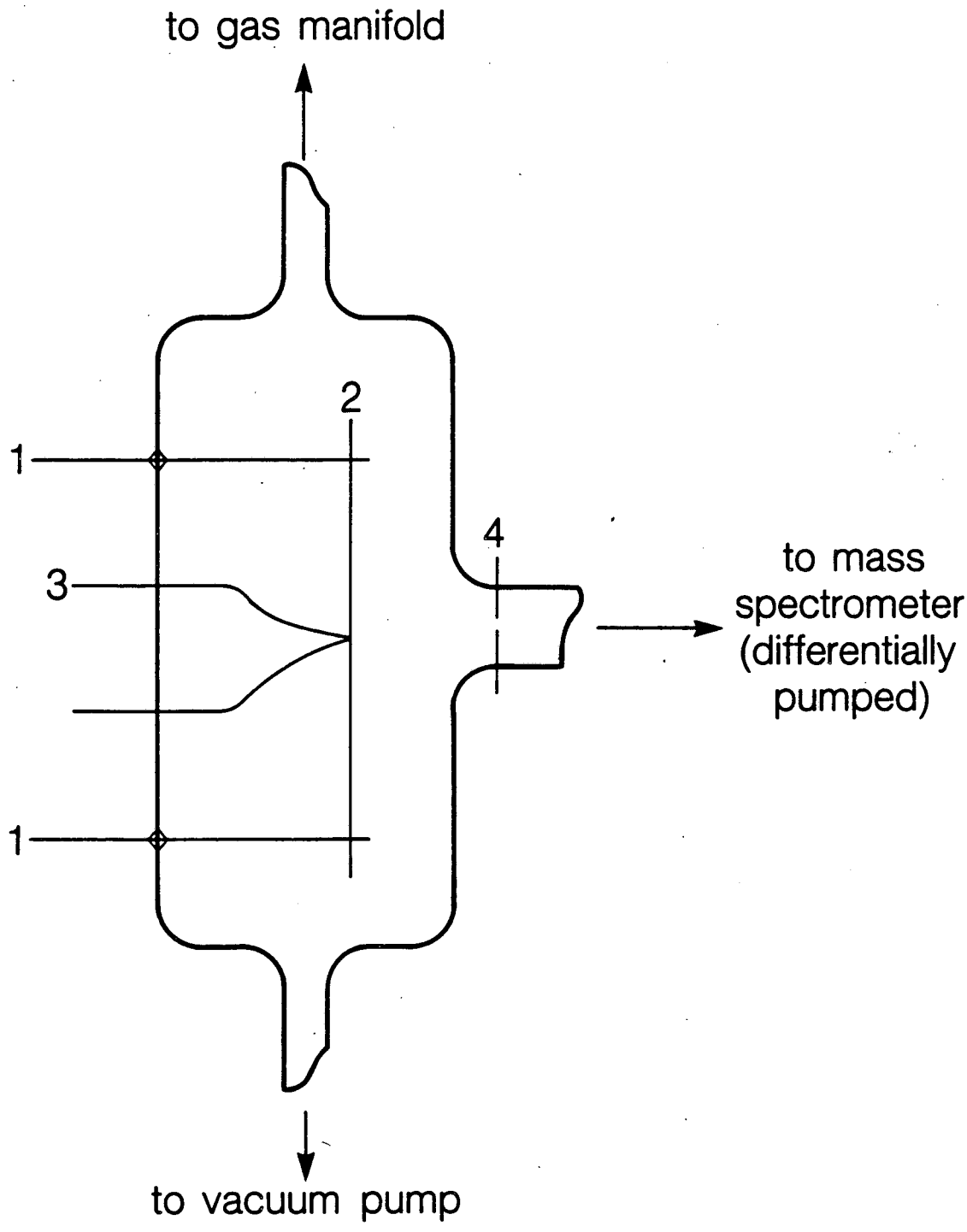

XBL 859-10743

Fig. 4

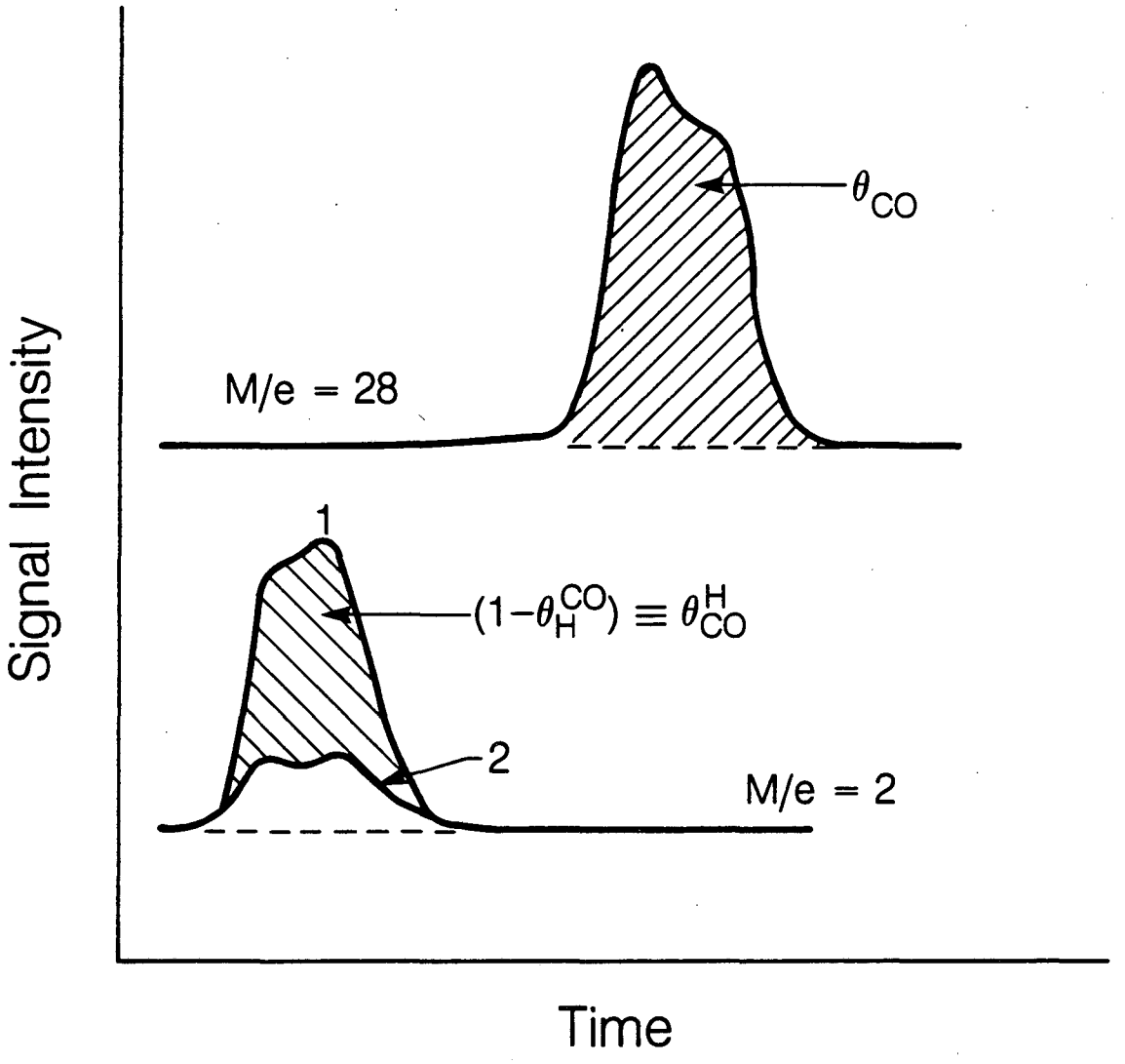

XBL 859-10746

Fig. 5

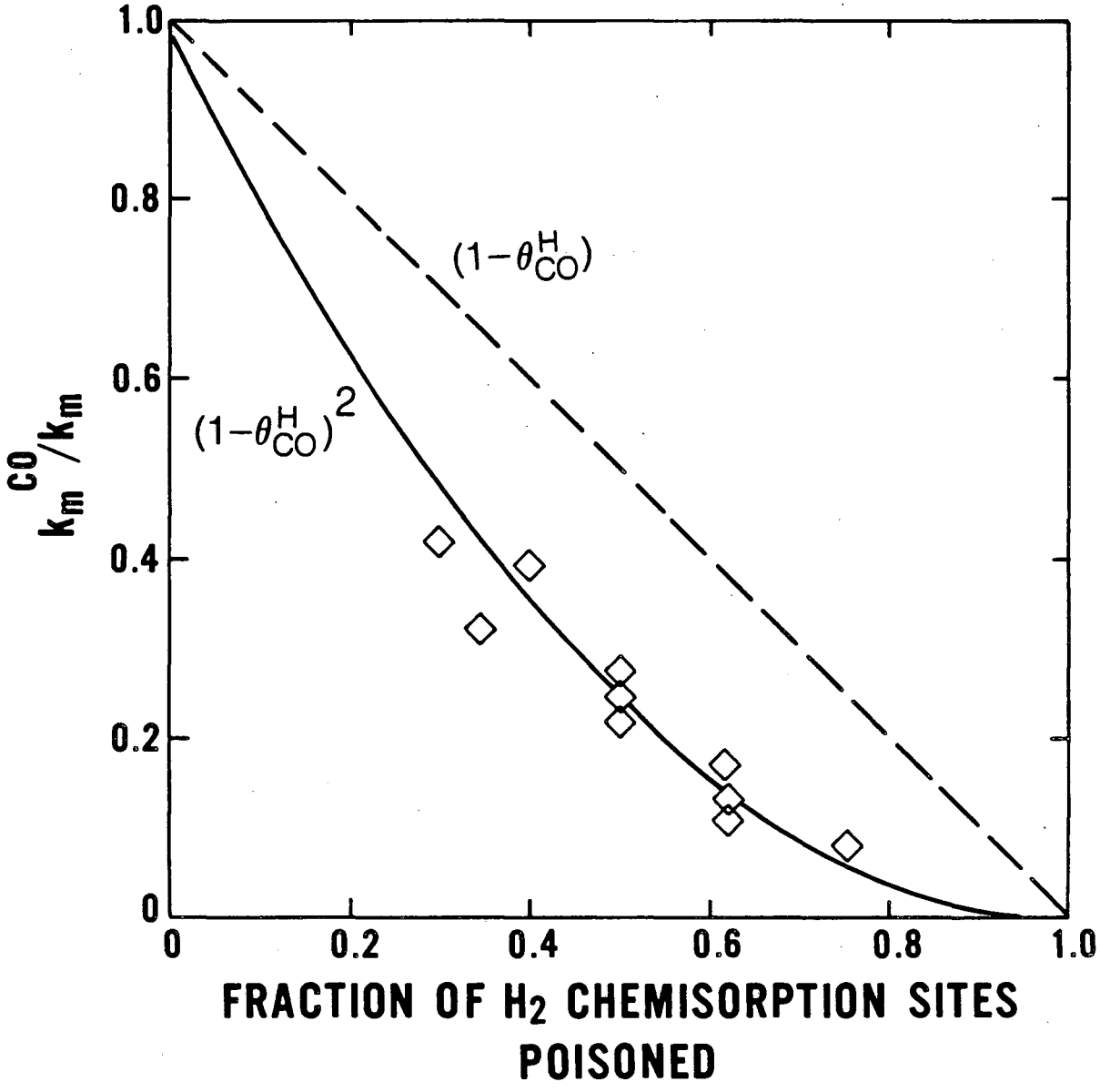

XBL 859-3987

Fig. 6

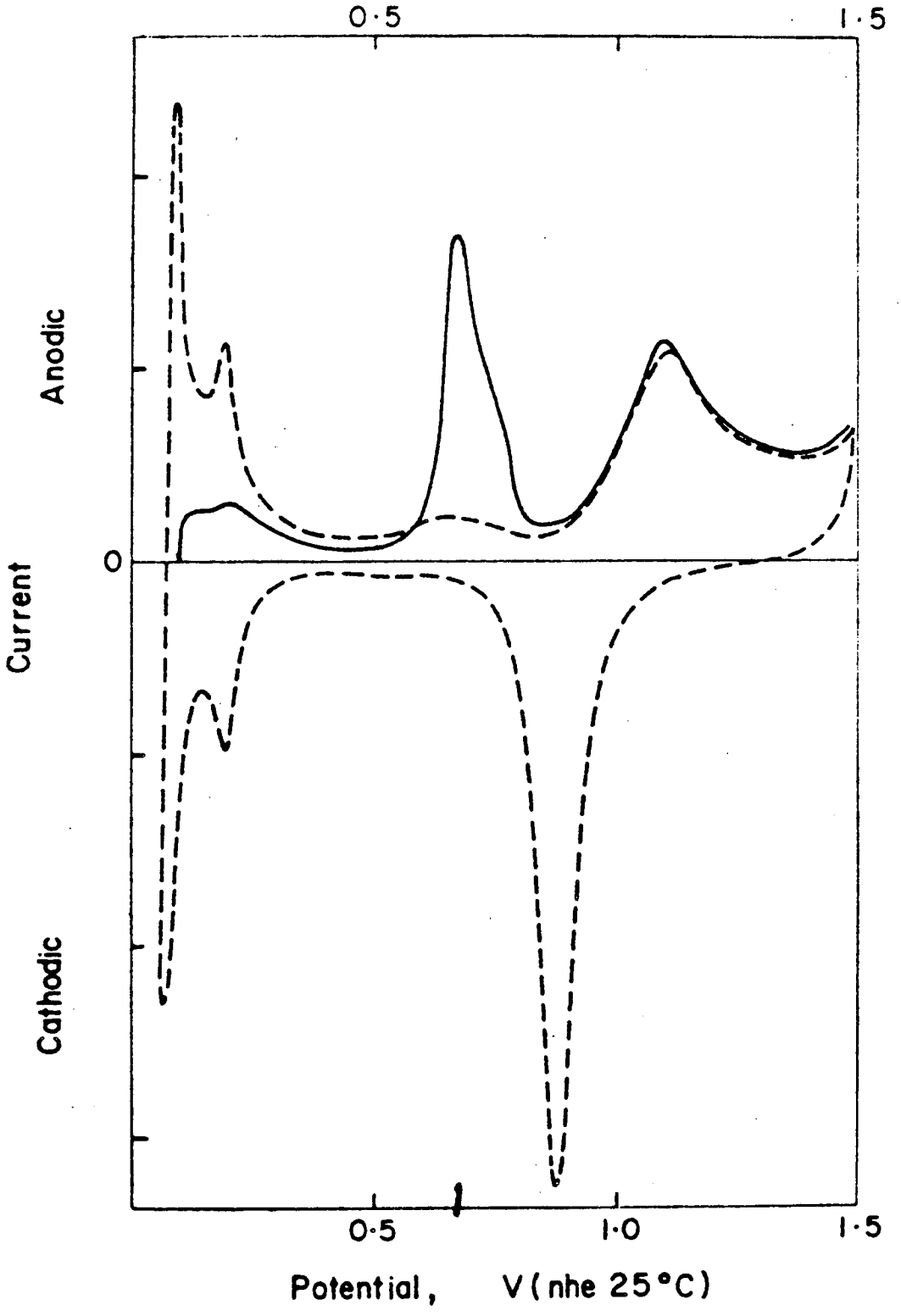

Fig. 7

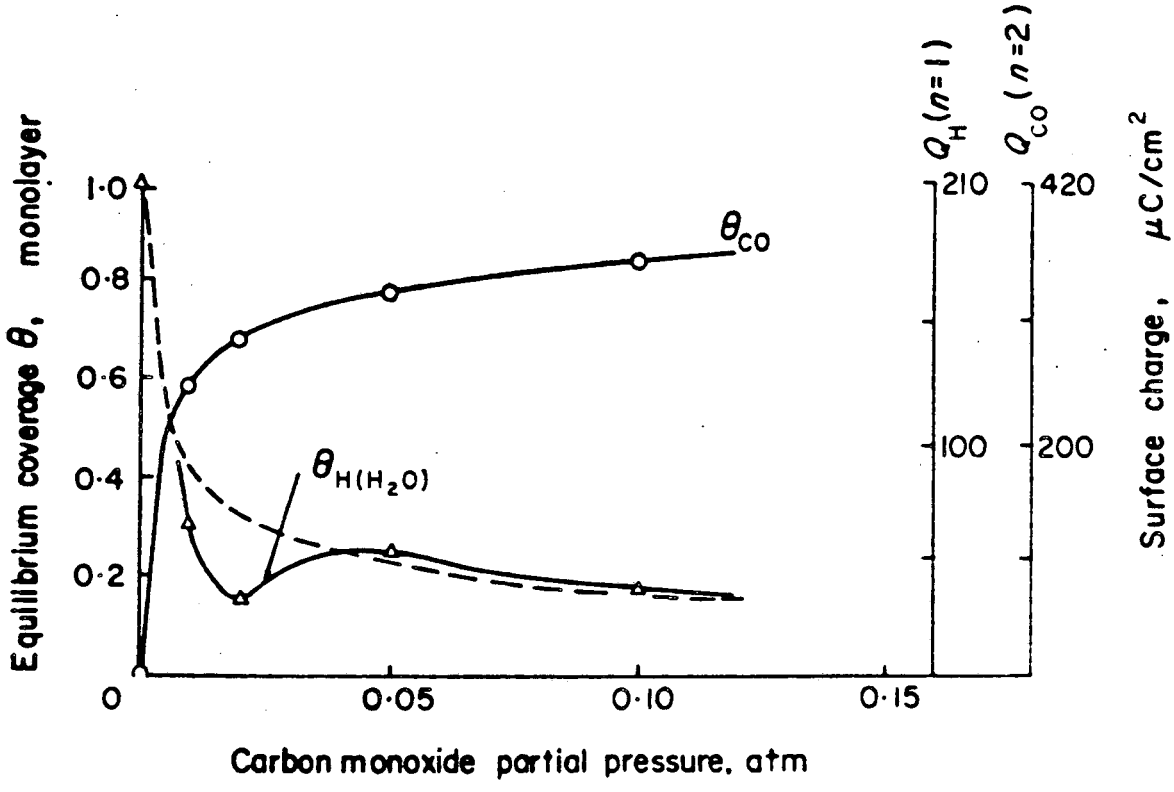
Equilibrium coverage θ, monolayer
1·0
0·8
0·6
0·4
0·2
0
0·05
0·10
0·15
Carbon monoxide partial pressure, atm
θCO
θH(H2O)
QH (n=1)
QCO (n=2)
210
100
420
200
Surface charge, μC/cm²

Fig. 8

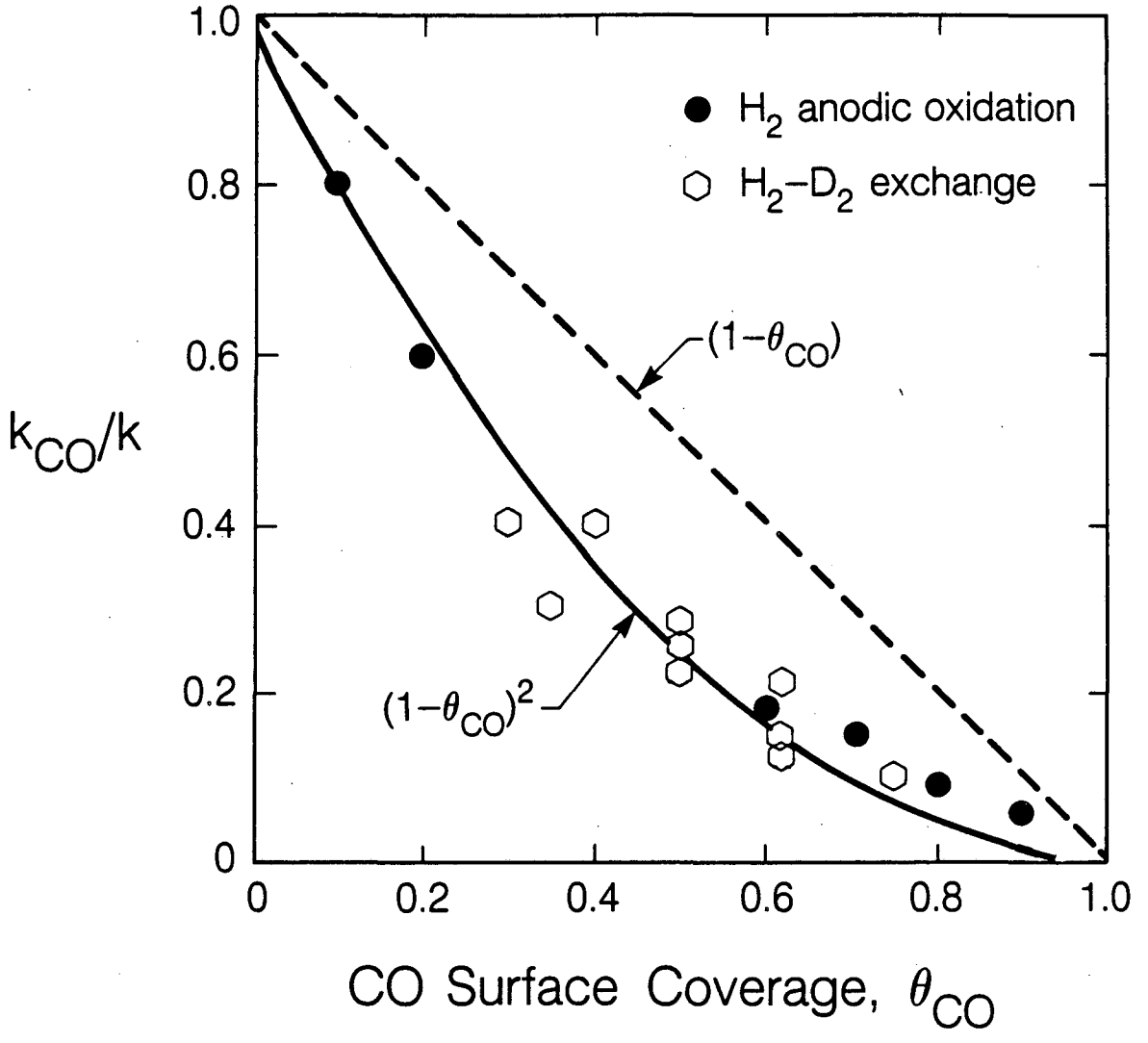

XBL 859-10747

Fig. 9

Ostwald Ripening

Conventional Catalyst:

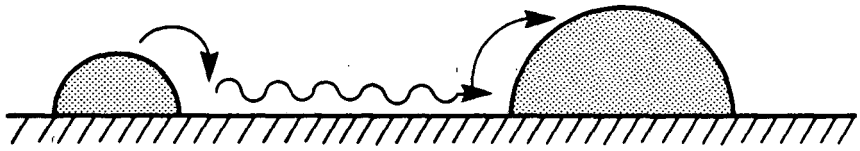

Electrocatalyst:

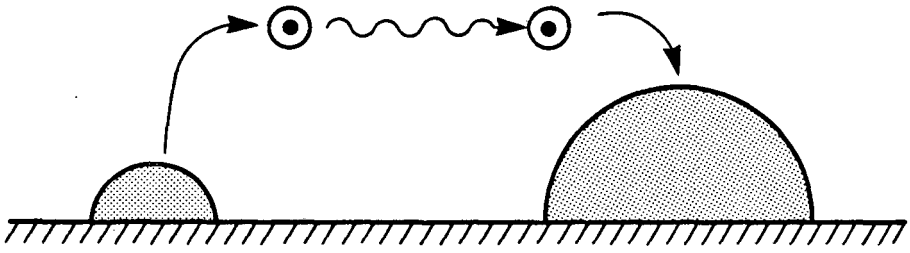

⊙ ≡ solvated metal ion

XBL 859-10745

Fig. 10

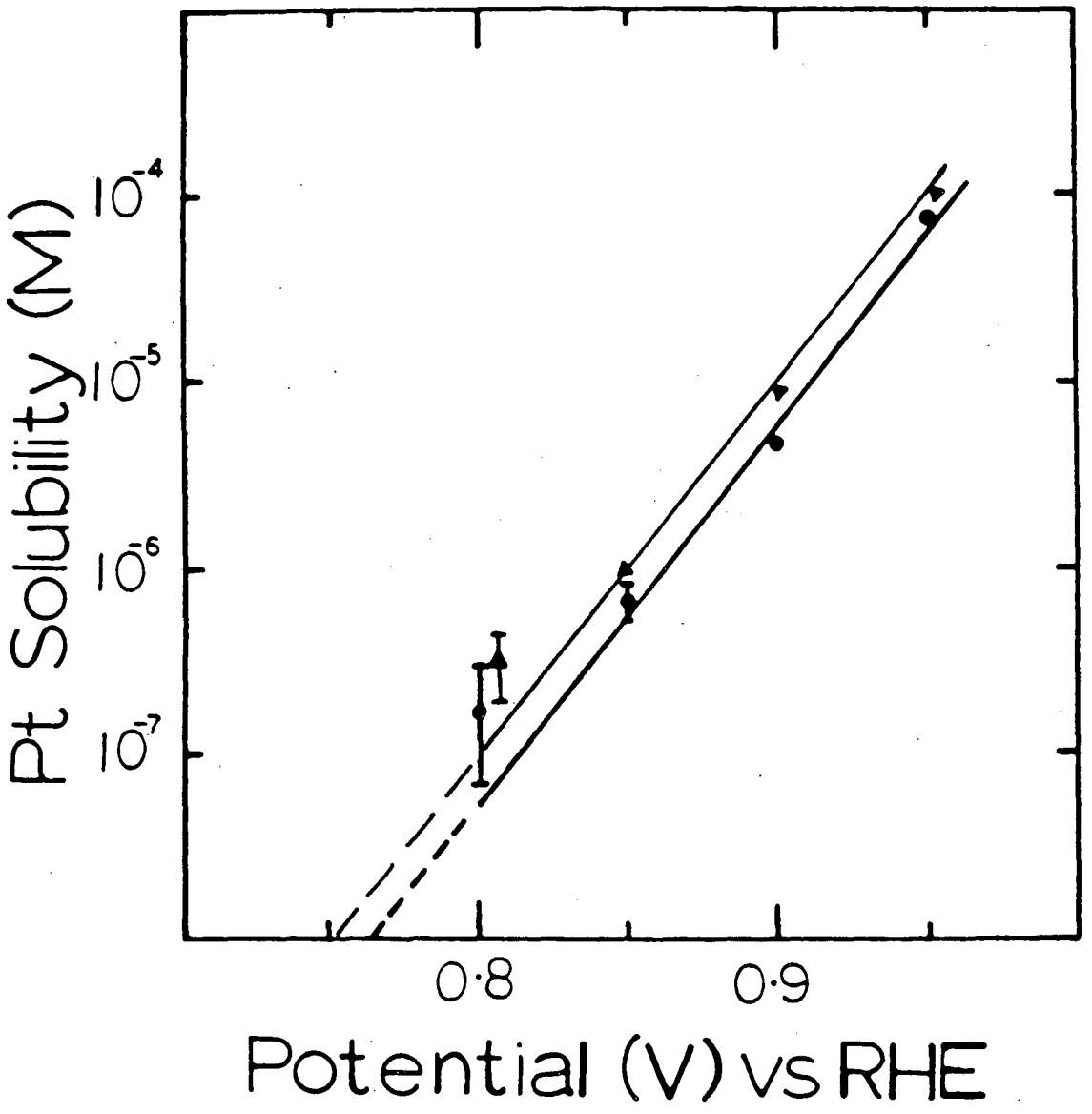

Fig. 11

Flux Calculations for Transport of Dissolved Pt Ions

Ostwald Ripening:

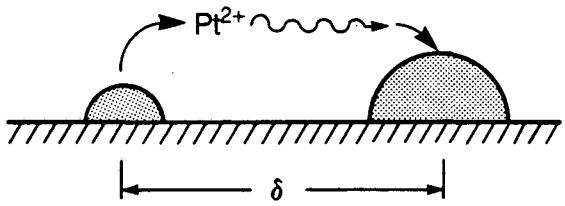

$N \simeq DC_0/\delta$, $\quad D \simeq 10^{-5}\ cm^2\ sec^{-1}$

$C_0 \simeq 10^{-8}$ M @ 0.75 V

$\delta \simeq 100$ Å

so $N \simeq 6\times10^{13}$ Pt atoms·cm^{-2}·sec^{-1} @ 0.75 V

Cathode-Anode Transfer:

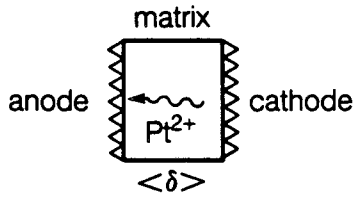

$D \simeq 10^{-5}\ cm^2\ sec^{-1}$

$C_0 \simeq 10^{-8}$ M @ 0.75

$\delta \simeq 0.1$ cm

so $N \simeq 7.2\times10^{-10}$ g Pt·cm^{-2}·hr^{-1} @ 0.75 V

XBL 859-10744

Fig. 12

This report was done with support from the Department of Energy. Any conclusions or opinions expressed in this report represent solely those of the author(s) and not necessarily those of The Regents of the University of California, the Lawrence Berkeley Laboratory or the Department of Energy.

Reference to a company or product name does not imply approval or recommendation of the product by the University of California or the U.S. Department of Energy to the exclusion of others that may be suitable.

LAWRENCE BERKELEY LABORATORY
TECHNICAL INFORMATION DEPARTMENT
UNIVERSITY OF CALIFORNIA
BERKELEY, CALIFORNIA 94720